The Embedded Boundary Integral Method (EBI) for the Incompressible Navier-Stokes equations

George Biros Lexing Ying and Denis Zorin

Courant Institute of Mathematical Sciences, New York University, NY 10012, USA

{biros,lexing,dzorin}@cs.nyu.edu

Abstract

We present a new method for the solution of the unsteady incompressible Navier-Stokes equations. Our goal is to achieve a robust and scalable methodology for two and three dimensional incompressible flows. The discretization of the Navier-Stokes operator is done using boundary integrals and structured-grid finite elements. We use finite-differences to advance the equations in time. The convective term is discretized via a semi-Lagrangian formulation which not only results in a spatial constant-coefficient (modified) Stokes operator, but in addition is unconditionally stable. The Stokes operator is inverted by a double-layer boundary integral formulation. Domain integrals are computed via finite elements with appropriate forcing singularities to account for the irregular geometry. We use a velocity-pressure formulation which we discretize with bilinear elements (Q1-Q1), which give equal order interpolation for the velocities and pressures. Stabilization is used to circumvent the div-stability condition for the pressure space. The integral equations are discretized by Nyström's method. For the specific approximation choices the method is second order accurate. Our code is built on top of PETSc, an MPI based parallel linear algebra library. We will present numerical results and discuss the performance and scalability of the method in two dimensions.

1 Introduction

In this article we propose a boundary integral method for the unsteady incompressible Navier-Stokes in complex geometries. Most state-of-the-art methods for such problems are based on local PDE-based formulations—finite element, finite difference or finite volume methods. These discretization techniques require unstructured or semi-structured meshes for local discretizations. For irregular domains, mesh generation is still a bottleneck—especially on multiprocessor platforms, three dimensions and for problems with moving boundaries.

Several researchers have used boundary integral formulations to model the homogeneous Stokes problem (no distributed forcing terms); see (Pozrikidis, 1992) for a detailed presentation of the formulation and derivation of boundary integral equations for potential and viscous flows. In (Gómez and Power, 1997; Mammoli and Ingber, 2000; Power, 1993), the homogeneous Stokes problem is solved via a primitive variable formulation (velocity and pressure), combined with multipole expansions to accelerate the matrix-vector multiplications.

Despite its effectiveness, a boundary integral formulation becomes less attractive for problems

with distributed forces. By the nature of the problem some kind of domain computations are required: domain convolution of the forcing term with the fundamental solution. These integrals are also known as *Newton potentials*. A problem with this approach is that the integration is a global operation. Fast multipole methods (FMM), (Greengard and Rokhlin, 1987), can be used to accelerate this calculation. A second problem is that the integrals are quite difficult to evaluate accurately for points close to the boundary—the kernels become nearly singular. Adaptive integration can be used but this complicates the computation.

Alternatively, the embedded boundary integral method (EBI) uses local methods, like finite elements, to efficiently evaluate the contribution from distributed forces. With the EBI method we embed the flow domain inside a larger domain, for which fast-scalable solvers are available (most likely a regular grid), and to which we suitably extend the velocity and pressure fields. We use an integral formulation to compute the inteface jumps of the velocity and its derivatives and then we use Taylor expansions to express these jumps as a source term at regular grid points close to the interface. This source term, which appears in the right hand side of a the regular grid problem, we term Taylor Expansion Stencil Correction (TESC). Depending on the details of the implementation the method can be first, second, or higher order accurate. EBI originally appeared in Anita Mayo's work (Mayo, 1984) for the Laplace and biharmonic operators.

In the following sections we discuss EBI method and its different algorithmic components. In Section 2 we give an overall description of the method; in Section 3 we explain the boundary integral formulation; in Section 4 we explain how the Taylor expansions stencil corrections are used to compute Newton potentials; and in 5 we present numerical results.

Notation. Scalars will be denoted with lowercase italics, vectors with lowercase boldface letters; tensors and matrices will be denoted with uppercase boldface letters. Infinitely dimensional quantities will be in italics, whereas finite dimensional ones (usually discretizations) will be non-italic fonts.

2 Description of the Embedded Boundary Integral method

We seek solutions for the incompressible Navier-Stokes equations inside multiply connected domain with Dirichlet boundary conditions. We choose a primitive variable formulation (velocities and pressures), for which the momentum and mass conservation laws are given by

$$\begin{aligned} \frac{\partial \boldsymbol{u}}{\partial t} + (\nabla \boldsymbol{u})\boldsymbol{u} - \nu \Delta \boldsymbol{u} + \nabla p = 0, \quad \text{in} \quad \omega \times (0,T], \\ \text{div}\boldsymbol{u} = \boldsymbol{0}, \quad \text{in} \quad \omega \times [0,T], \\ \boldsymbol{u} = \boldsymbol{g}, \quad \text{on} \quad \gamma \times (0,T]. \end{aligned} \tag{1}$$

Here $\boldsymbol{u}$ is the velocity field, p is the pressure, and $\boldsymbol{g}$ is a given Dirichlet boundary condition for the velocity. To circumvent the nonlinearity of the convective term we use a semi-Lagrangian formulation (Douglas Jr. and Russell, 1982). The relation between the the Lagrangian and Eulerian description of the acceleration term is given by

$$\frac{d\boldsymbol{u}}{dt} = \frac{\partial \boldsymbol{u}}{\partial t} + (\nabla \boldsymbol{u})\boldsymbol{u}. \tag{2}$$

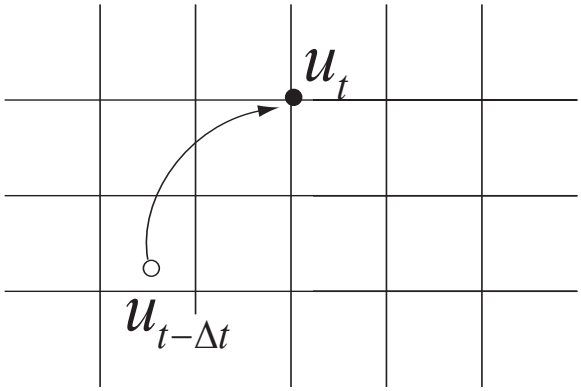

Figure 1: Semi-Lagrangian formulation. To discretize in time we have to locate the point from which a particle with velocity $\boldsymbol{u}(t-\Delta t)$ traveled to the grid point with velocity $\boldsymbol{u}(t)$.

We discretize the left hand side, using a backward Euler scheme:

$$\frac{d\boldsymbol{u}(\mathbf{x}(t),t)}{dt} = \frac{1}{\Delta t}(\boldsymbol{u}(\mathbf{x}(t),t) - \boldsymbol{u}(\mathbf{x}(t-\Delta t),t-\Delta t). \tag{3}$$

For a semi-Lagrangian formulation $\mathbf{x}(t)$ will always be a some point of the regular grid. To compute the velocity at the previous time step, we have to compute $\mathbf{x}(t-\Delta t)$; i.e. we have to locate the starting point of the flow particle that arrived to the grid point $\mathbf{x}$, (Figure 2). To compute $\mathbf{x}(t-\Delta t)$ we use

$$\frac{d\mathbf{x}(t)}{dt} = \boldsymbol{u}(\mathbf{x}(t),t). \tag{4}$$

If $\delta\mathbf{x}$ is $\mathbf{x}(t) - \mathbf{x}(t-\Delta t)$, we obtain the following nonlinear equation (for $\delta\mathbf{x}$)

$$\delta\mathbf{x} = \Delta t\boldsymbol{u}(\mathbf{x}(t) - \delta\mathbf{x}, t-\Delta t), \tag{5}$$

and which we solve iteratively by taking a few Piccard steps. The interpolation of $\boldsymbol{u}$ has to be done carefully to avoid excessive dissipation. We use cubic b-splines.

After the time discretization we obtain a system of the form

$$\begin{aligned} \alpha\boldsymbol{u} - \nu\Delta\boldsymbol{u} + \nabla p &= \boldsymbol{b}, \quad \text{in} \quad \omega, \\ \text{div}\boldsymbol{u} &= \mathbf{0}, \quad \text{in} \quad \omega, \\ \boldsymbol{u} &= \boldsymbol{g}, \quad \text{on} \quad \gamma. \end{aligned} \tag{6}$$

Here $\boldsymbol{b}$ is a body force and includes the terms from the time stepping. As explained in the introduction, in order to avoid the cost of mesh generation, we would like to solve the above equations via a boundary integral formulation. However the presence of the forcing term $\boldsymbol{b}$ significantly complicates this approach.

Anita Mayo's algorithm can be viewed as a method to evaluate Newton potentials accurately and inexpensively. We first embed ω in a regular (or more generally, easier to discretize) domain Ω and by linearity we decompose (6) into two problems: a problem that has an inhomogeneous

distributed (or body) force and homogeneous boundary conditions (*particular solution*)

$$\begin{aligned} \alpha \boldsymbol{u}_1 - \nu \Delta \boldsymbol{u}_1 + \nabla p_1 &= \boldsymbol{b}, \quad \text{in} \quad \Omega \\ \text{div} \boldsymbol{u}_1 &= \boldsymbol{0}, \quad \text{in} \quad \Omega, \\ \boldsymbol{u}_1 &= \boldsymbol{0}, \quad \text{on} \quad \Gamma; \end{aligned} \tag{7}$$

and a problem that satisfies the boundary conditions (*homogeneous solution*)

$$\begin{aligned} \alpha \boldsymbol{u}_2 - \nu \Delta \boldsymbol{u}_2 + \nabla p_2 &= \boldsymbol{0}, \quad \text{in} \quad \omega, \\ \text{div} \boldsymbol{u}_2 &= \boldsymbol{0}, \quad \text{in} \quad \omega, \\ \boldsymbol{u}_2 &= \boldsymbol{g} - \boldsymbol{u}_1, \quad \text{on} \quad \gamma. \end{aligned} \tag{8}$$

We solve (7) with a $Q1 - Q1$ finite-element approximation method. For the second problem we use a double layer boundary integral formulation.

The solution ($\boldsymbol{u}$, p) is given by $\boldsymbol{u}_1 + \boldsymbol{u}_2$ and $p = p_1 + p_2$. The evaluation ($\boldsymbol{u}_2$, p_2) for a point inside ω can be done with convolution of double layer kernels with the velocity potential. This presents the same difficulties with the convolution of a forcing term. An easier way to compute $\boldsymbol{u}_2$ is based on the fact that once problems (7) and (8) are solved, derivatives of the solution $\boldsymbol{u}$ can be very accurately computed on γ. A discontinuous extension of $\boldsymbol{u}_2$ on Ω can be chosen so that all the interface jumps can be semi-analytically computed. By tracking the intersection of the interface with the background grid and using the jump relations, we employ Taylor expansions to correct the stencil truncation error (TESCs). Using TESCs this information is transformed into a distributed force $\boldsymbol{s}$ which can be also viewed as the discretization of a dipole along the boundary. Then we solve

$$\begin{aligned} \alpha \boldsymbol{u}_3 - \nu \Delta \boldsymbol{u}_3 + \nabla p_3 &= \boldsymbol{s}_u, \quad \text{in} \quad \Omega \\ \text{div} \boldsymbol{u}_3 &= \boldsymbol{s}_p, \quad \text{in} \quad \Omega, \\ \boldsymbol{u}_3 &= \boldsymbol{u}_2, \quad \text{on} \quad \Gamma; \end{aligned} \tag{9}$$

where (at the limit) $\boldsymbol{u}_3$ is discontinuous on γ, and $\boldsymbol{u}_2$ is the restriction of $\boldsymbol{u}_3$ in ω.

Therefore, an EBI solve consists of two regular grid solves and one boundary integral solve.

3 The Double Layer Formulation for the Stokes Equations

In this section we examine a problem of the form (6) with $\boldsymbol{b} = \boldsymbol{0}$. We also assume that $\omega \subset \mathbb{R}^2$ is bounded and of C^2-class. We use an indirect formulation based on double layer potentials. For the steady Stokes operator the double layer potential is given by

$$\mathcal{D}[\boldsymbol{w}](\mathbf{x}) := \int_\gamma \mathcal{D}(\mathbf{x}, \mathbf{y}) \boldsymbol{w}(\mathbf{y}) \, d\gamma(\mathbf{y}) = \frac{1}{\pi} \int_\gamma \frac{\mathbf{r} \otimes \mathbf{r}}{\rho^2} \frac{\mathbf{r} \cdot \boldsymbol{n}(\mathbf{y})}{\rho^2} \boldsymbol{w}(\mathbf{y}) \, d\gamma(\mathbf{y}), \tag{10}$$

where $\boldsymbol{n}(\mathbf{y})$ is the outward surface normal at a boundary point $\mathbf{y}$. The unsteady potential is given by

$$\mathcal{D}_u[\boldsymbol{w}](\mathbf{x}) := \mathcal{D}[\boldsymbol{w}](\mathbf{x}) + \mathcal{D}_a[\boldsymbol{w}](\mathbf{x}), \tag{11}$$

with

$$\begin{aligned}\mathcal{D}_a[\boldsymbol{w}](\mathbf{x}) &= \int_\gamma \mathcal{D}_a(\mathbf{x},\mathbf{y})\, d\gamma(\mathbf{y}) = \\ &= \frac{1}{\pi}\int_\gamma v_1(\sigma)\Big(\frac{\boldsymbol{n}(\mathbf{y})\otimes\mathbf{r}}{\rho^2} + \frac{\mathbf{r}\cdot\boldsymbol{n}(\mathbf{y})}{\rho^2}\mathbf{I}\Big)\boldsymbol{w}(\mathbf{y}) \\ &\qquad + v_2(\sigma)\frac{\mathbf{r}\otimes\mathbf{r}}{\rho^2}\frac{\mathbf{r}\cdot\boldsymbol{n}(\mathbf{y})}{\rho^2}\boldsymbol{w}(\mathbf{y}) \\ &\qquad + v_3(\sigma)\frac{\mathbf{r}\otimes\boldsymbol{n}(\mathbf{y})}{\rho^2}\boldsymbol{w}(\mathbf{y})\, d\gamma(\mathbf{y}). \end{aligned} \tag{12}$$

Here σ is given by

$$\sigma = \rho\sqrt{\alpha}, \tag{13}$$

To define v_1, v_2, v_3 let us first use K_0 and K_1 for the modified Bessel functions of second kind of zero and first order respectively. We also define an auxiliary function $\beta(\sigma)$ by

$$\beta(\sigma) = \frac{1}{\sigma^2} + K_0(\sigma) + \frac{2K_1(\sigma)}{\sigma}. \tag{14}$$

Then

$$v_1(\sigma) = \frac{2\beta(\sigma) + \sigma K_1(\sigma)}{2}, \tag{15}$$

$$v_2(\sigma) = -4\beta(\sigma) - \sigma K_1(\sigma) - 1, \tag{16}$$

$$v_3(\sigma) = \frac{2\beta(\sigma) + 1}{2}. \tag{17}$$

For a derivation of the above formulas see (Pozrikidis, 1992).

We limit our discussion to the simply connected interior Dirichlet problem. The extension of EBI to exterior and Neumann problems is very similar to the interior problem. We can write the velocities as boundary potentials:

$$\boldsymbol{u}(\mathbf{x}) = \mathcal{D}[\boldsymbol{\mu}](\mathbf{x}), \quad \mathbf{x} \ \text{ in } \ \omega, \tag{18}$$

$$p(\mathbf{x}) = \mathcal{K}[\boldsymbol{\mu}](\mathbf{x}), \quad \mathbf{x} \ \text{ in } \ \omega. \tag{19}$$

Here $\boldsymbol{\mu}$ is the hydrodynamic potential, and $\mathcal{K}$ is defined by:

$$\mathcal{K}[\boldsymbol{w}](\mathbf{x}) := \int_\gamma \mathcal{K}(\mathbf{x},\mathbf{y})\cdot\boldsymbol{w}(\mathbf{y})\, d\gamma(\mathbf{y}) = -\nu\frac{1}{\pi}\int_\gamma \frac{1}{\rho^2}(\mathbf{I} - 2\frac{\mathbf{r}\otimes\mathbf{r}}{\rho^2})\boldsymbol{n}(\mathbf{y})\cdot\boldsymbol{w}(\mathbf{y})\, d\gamma(\mathbf{y}). \tag{20}$$

Taking limits to the boundary from the interior and exterior regions we obtain

$$\boldsymbol{u}(\mathbf{x}) = -\frac{1}{2}\boldsymbol{\mu}(\mathbf{x}) + \mathcal{D}[\boldsymbol{\mu}](\mathbf{x}), \quad \mathbf{x} \ \text{ on } \ \gamma. \tag{21}$$

A necessary condition for a solution of the above equation is that $\boldsymbol{u}$ has to satisfy

$$\int_\gamma \boldsymbol{u}\cdot\boldsymbol{n}\, d\gamma = 0, \tag{22}$$

which a direct consequence of the conservation of mass. This constraint is an indication that for the simply-connected interior problem the double layer operator has a null space of dimension at least one. In fact, it can be shown ((Power and Wrobel, 1995), p. 159) that the dimension of the null space is exactly one. The null space can be removed by a rank-one modification ((Power and Wrobel, 1995), p. 615). Let

$$\mathcal{N}[\boldsymbol{w}](\mathbf{x}) := \int_\gamma \mathcal{N}(\mathbf{x},\mathbf{y})\boldsymbol{w}(\mathbf{y})\, d\gamma(\mathbf{y}) = \int_\gamma \boldsymbol{n}(\mathbf{x}) \otimes \boldsymbol{n}(\mathbf{y})\boldsymbol{w}(\mathbf{y})\, d\gamma(\mathbf{y}); \tag{23}$$

we solve for $\boldsymbol{u}$ from

$$\boldsymbol{u}(\mathbf{x}) = -\frac{1}{2}\boldsymbol{\mu}(\mathbf{x}) + \mathcal{D}[\boldsymbol{\mu}](\mathbf{x}) + \mathcal{N}[\boldsymbol{\mu}](\mathbf{x}), \quad \mathbf{x} \ \text{ on } \ \gamma. \tag{24}$$

For the multiply connected interior problem, a direct calculation can verify that the steady double layer kernel has a larger null space—spanned by potentials that correspond to restrictions of rigid body motion velocity fields on the boundary. These fields generate zero boundary tractions and thus belong to the null space of the double layer kernel. In (Power, 1993) point singularities are used to complete the spectrum of the double layer operator.

We discretize (24) by the Nyström method combined with the composite trapezoidal rule which achieves superalgebraic convergence for smooth data. (Without loss of generality we assume ω to be simply connected in the remaining part of this section.) Let $[0, 2\pi]$ be the curve parameterization space and n the number of discretization points with $h = 2\pi/n$. We discretize by:

$$\boldsymbol{u}(\mathbf{x}(ih)) = -0.5\boldsymbol{\mu}(ih) + \sum_{j=1}^{n} \mathcal{D}(\mathbf{x}(ih),\mathbf{y}(jh))\boldsymbol{\mu}(\mathbf{y}(jh))\, \|\nabla\mathbf{y}(jh)\|_2 \tag{25}$$

$$+ \boldsymbol{n}(\mathbf{x}(ih)) \sum_{j=1}^{n} \boldsymbol{\mu}(\mathbf{y}(jh)) \cdot \boldsymbol{n}(\mathbf{y}(jh)\, \|\nabla\mathbf{y}(jh)\|_2, \quad i = 1,\ldots,n. \tag{26}$$

which results in a dense $2n \times 2n$ linear system. Here $\mathbf{y}(\cdot)$ is the parameterization of γ.

Jump computation. Equation (18) is defined for points inside ω. We can use exactly the same relation to extend $\boldsymbol{u}$ in $\mathbb{R}^2/\bar{\omega}$. The resulting field is discontinuous across the inteface. From the properties of the double layer kernel (for an interior problem) we have the following jump relations:

$$\begin{aligned} \boldsymbol{u}_e - \boldsymbol{u}_i &= \boldsymbol{\mu}, \\ \boldsymbol{\sigma}_e - \boldsymbol{\sigma}_i &= 0, \\ (\nabla\boldsymbol{u}_e - \nabla\boldsymbol{u}_i)\boldsymbol{t} &= \dot{\boldsymbol{\mu}}. \end{aligned} \tag{27}$$

The left hand side formulas should be interpreted as appropriate limits from the exterior and interior of the domain. The last equation can be obtained by differentiating the first equation in the tangential direction;$\dot{\boldsymbol{\mu}}$ is the derivative of the potential with respect the parameterization of the curve: $\dot{\boldsymbol{\mu}} = d\boldsymbol{\mu}(\mathbf{y}(t))/dt$. Similar relations can be derived for the pressure. Higher order derivatives can be obtained by differentiating (27) augmented with the continuity of the momentum equation across the interface.

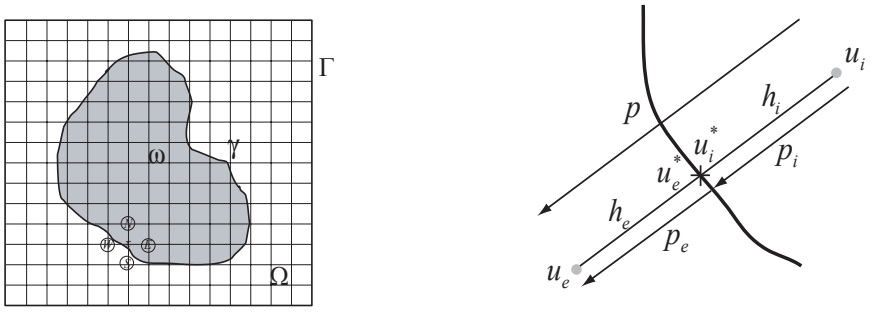

(a) (b)

Figure 2: Stencil corrections. Given a irregular domain ω we embedded in a regular or fictitious domain Ω. A finite difference scheme can be used to approximate an elliptic operator. For stencils that cross the interface, like the one depicted in (c), the truncation error is constant as the mesh size goes to zero. If one knows $u_e - u_i$ appropriate correction terms can be computed so that a converging scheme is obtained.

4 Taylor Expansion Stencil Corrections

In this section we show how discontinuities across the interface (jumps) can be used as a forcing term for an equivalent problem in a regular grid. For simplicity we consider Poisson's equation $\Delta u = b$, in ω with Dirichlet boundary conditions on γ (Fig. 4). We embed ω in a larger domain Ω and assume that u will be discontinuous across the inteface γ.

We also assume that the discontinuities (jump conditions) are known up to second derivatives. Typical discretizations of elliptic PDE's (finite elements, finite differences or finite volumes) produce a "stencil", a formula that relates each discretization variable u_i to its spatial neighbors. This relation can be expressed by

$$\alpha u_i + \sum_j \beta_j u_j = \zeta b_i,$$

where j runs through the neighbors of u_i. (For unstructured grids α, β, ζ and the number of neighbors depends on i.) A standard technique in the finite-differences literature is to use Taylor expansions of the neighbors to determine the truncation error. For the standard 2D five-point discrete Laplacian (Fig. 4(c)) the stencil is:

$$\frac{1}{4}u_i - \sum_{j=1}^{4} u_j = h^2 b_i, \tag{28}$$

where h is the mesh size.

In the absence of an interface this stencil is well defined and second order accurate. For stencils that intersect with the interface, however, this is not true. For example in Fig. 4(c) the stencil around point X includes two points, W and S for which a Taylor expansion will not work since u and its derivatives are not continuous across the interface.

In Fig. 4(d), we show an example for which two unknowns u_i and u_e are related in a discretization stencil that "crosses" the interface at point X. The limit from the interior is denoted as u_i^* and

the limit from the exterior is denoted as u_e^*. The key idea is that the truncation error of the stencil can be corrected to be second (or higher-order) accurate if we just know the difference between the interface limits, and not their exact values.

For this section, let us define D as the Gateaux derivative operator, and

$$\begin{aligned} \mu &= u_e^* - u_i^*, \\ \boldsymbol{D}\mu &= \boldsymbol{D}u_e^* - \boldsymbol{D}u_i^*, \\ \boldsymbol{D}^2\mu &= \boldsymbol{D}^2u_e^* - \boldsymbol{D}^2u_i^*, \end{aligned} \tag{29}$$

the jump conditions up to second derivatives. Let us also define $\boldsymbol{n} = \boldsymbol{p}/h$ (not to be confused with the normal to the interface) to be the unit-length direction vector oriented from u_i to u_e, $p_e = h_e\boldsymbol{n}$ and $p_i = h_i\boldsymbol{n}$, Fig. 4(d). By using Taylor expansions we can write

$$\begin{aligned} u_e &= u_e^* + h_e\boldsymbol{D}u_e^* \cdot \boldsymbol{n} + \frac{h_e^2}{2}\boldsymbol{n} \cdot (\boldsymbol{D}^2u_e^*)\boldsymbol{n} + \mathcal{O}(h^3) \\ &= (\mu + u_i^*) + h_e(\boldsymbol{D}\mu + \boldsymbol{D}u_i^*) \cdot \boldsymbol{n} + \frac{h_e^2}{2}\boldsymbol{n} \cdot (\boldsymbol{D}^2\mu + \boldsymbol{D}^2u_i^*)\boldsymbol{n} + \mathcal{O}(h^3). \end{aligned} \tag{30}$$

If we define

$$s_i = \mu + h_e\boldsymbol{D}\mu \cdot \boldsymbol{n} + \frac{h_e^2}{2}\boldsymbol{n} \cdot (\boldsymbol{D}^2\mu)\boldsymbol{n} \tag{31}$$

then (30) becomes

$$u_e = s_i + u_i^* + h_e\boldsymbol{n} \cdot \boldsymbol{D}^2u_i^* + \frac{h_e^2}{2}\boldsymbol{n} \cdot (\boldsymbol{D}^2u_i^*)\boldsymbol{n} + \mathcal{O}(h^3).$$

Next we expand u_i^* around u_i to get

$$\begin{aligned} u_e &= s_i + u_i + h_i\boldsymbol{n} \cdot \boldsymbol{D}u_i + \frac{h_i^2}{2}\boldsymbol{n} \cdot (\boldsymbol{D}^2u_i)\boldsymbol{n} \\ &\quad + h_e(\boldsymbol{D}u_i + h_i(\boldsymbol{D}^2u_i)\boldsymbol{n}) \cdot \boldsymbol{n} + \frac{h_e^2}{2}\boldsymbol{n} \cdot (\boldsymbol{D}^2u_i)\boldsymbol{n} + \mathcal{O}(h^3) \\ &= u_i + h\boldsymbol{D}u_i \cdot \boldsymbol{p} + \frac{h}{2}\boldsymbol{p} \cdot (\boldsymbol{D}^2u_i)\boldsymbol{p} + s_i + \mathcal{O}(h^3). \end{aligned} \tag{32}$$

Similarly (take a minus sign for the opposite direction vectors and a minus sign for the jump) we can write

$$u_i = u_e - h\boldsymbol{D}u_e \cdot \boldsymbol{p} + \frac{h^2}{2}\boldsymbol{p} \cdot (\boldsymbol{D}^2u_e)\boldsymbol{p} + s_e + \mathcal{O}(h^3), \tag{33}$$

where s_e is given by:

$$s_e = -(\mu - h_i\boldsymbol{D}\mu \cdot \boldsymbol{n} + \frac{h_i^2}{2}\boldsymbol{n} \cdot (\boldsymbol{D}^2\mu)\boldsymbol{n}). \tag{34}$$

For the stencil centered at u_e we use (34) and for the stencil centered at u_i we use (31).

By using the correction term we achieve $\mathcal{O}(h^3)$ truncation error for a second order discretization of the Laplacian for the points immediate to the boundary and $\mathcal{O}(h^4)$ for the remaining set of points. This results to an $\mathcal{O}(h^2)$ discretization error for all points (Mayo, 1984). Second order convergence can be achieved using jump information up to second derivatives.

5 Numerical Experiments

We have chosen to solve for the velocity and pressure simultaneously using a finite element method with $Q1$-$Q1$ bilinear elements. The $Q1$-$Q1$ element does not satisfy the $\inf$-$\sup$ condition (Gunzburger, 1989). In (Norburn and Silvester, 1999) it is shown how to optimally stabilize by adding a pressure diffusion term which is proportional to the viscosity and to the square of the mesh size. The resulting approximation is second order accurate for the velocities and first order accurate for the pressures. In this section we test EBI on a problem with exact analytic solution.

We present preliminary results for the unsteady Stokes and Navier-Stokes problems. We have chosen an synthetic solution for the steady Stokes given by

$$\boldsymbol{u} = 2\left\{-x^2y, y^2x\right\},\ p = \sin(xy),\ \boldsymbol{b} = 4\nu\left\{y(1+\cos(xy), -x(1+\cos(xy)\right\}.$$

We use the unsteady solver to "march" to the steady state solution. In Figures 3 and 4 we show the exact solution and the error distribution for a 64^2 and a 256^2 grid respectively. Pointwise

Figure 3: Solution and error for the for the 64^2 grid.

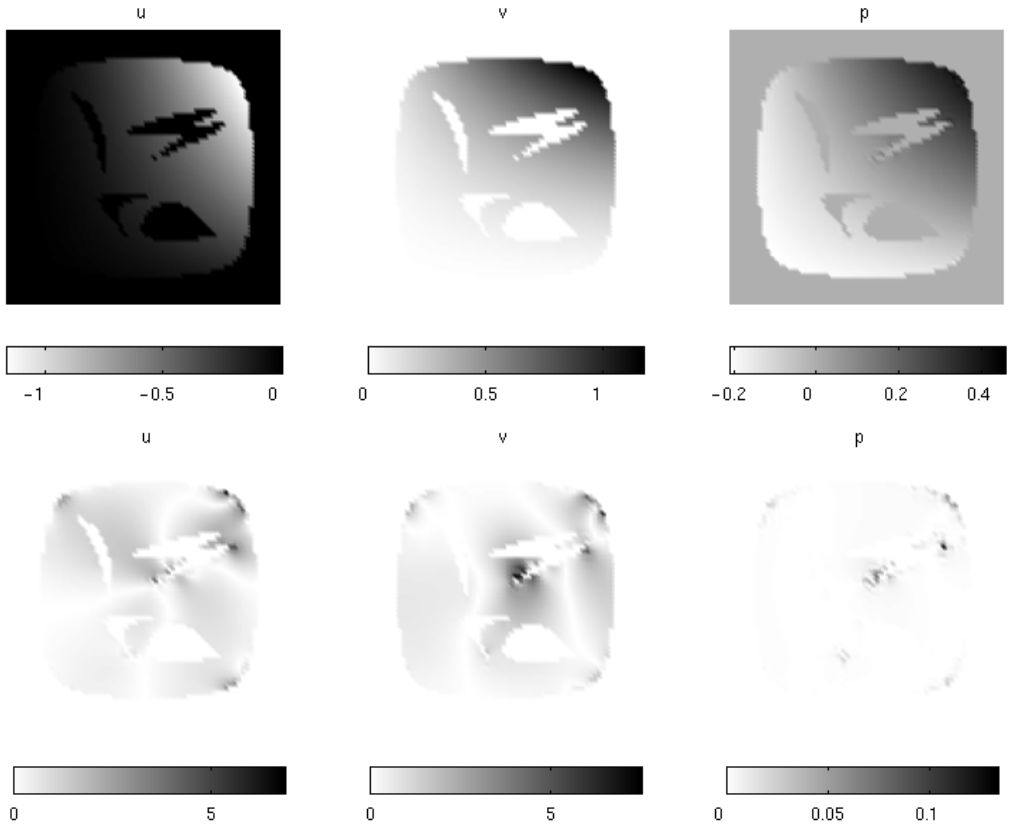

error norms for the first-order and second-order accurate jump corrections are given in Table 1. The first and second columns give the maximum pointwise absolute errors for the velocity and pressure; and the third and fourth columns give results for second order accurate jumps. We can

Figure 4: Solution and error for the for the 256^2 grid.

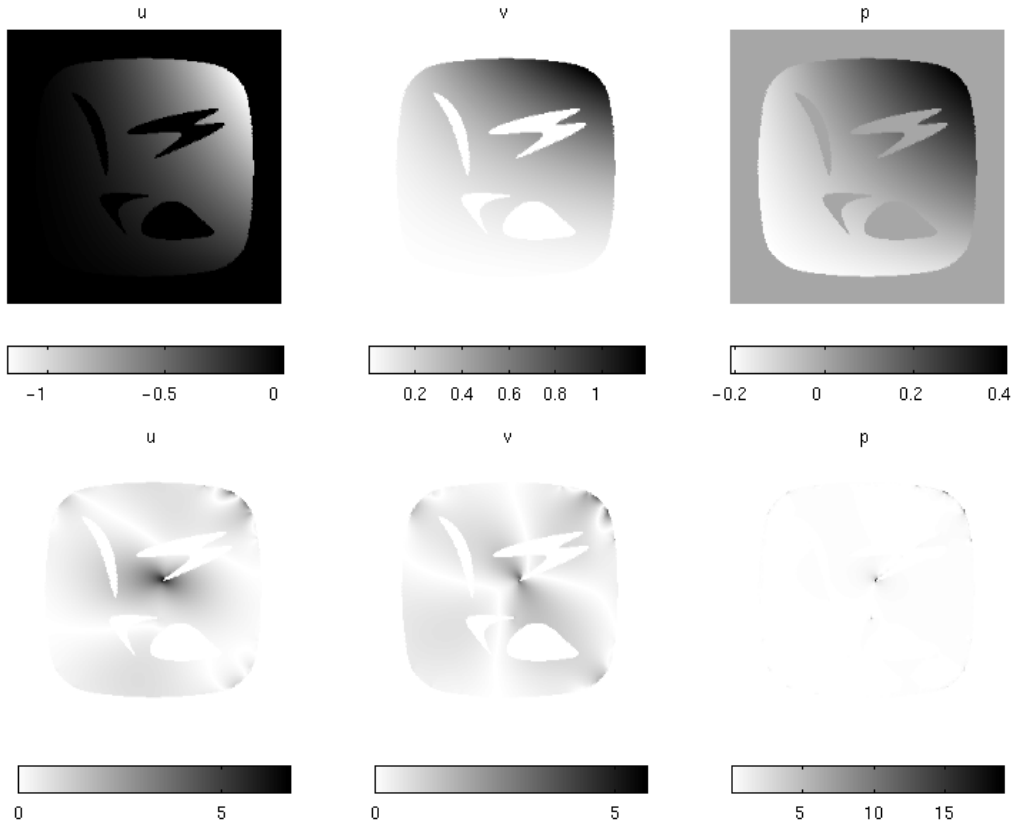

observe suboptimal rates for the first-order jumps and optimal convergence rates for the second order jumps. For this type of flow the influence of the time stepping accuracy is negligible.

Table 1: Pointwise absolute error for the velocity and pressure.

	first-order		*second-order*	
grid size	u_{err}	p_{err}	u_{err}	p_{err}
32^2	1.38×10^{-1}	9.82×10^{-1}	4.19×10^{-3}	1.56×10^{-1}
64^2	4.98×10^{-2}	7.86×10^{-1}	1.51×10^{-3}	7.91×10^{-2}
128^2	1.49×10^{-2}	4.38×10^{-1}	4.68×10^{-4}	4.78×10^{-2}
256^2	5.65×10^{-3}	3.57×10^{-1}	1.18×10^{-4}	2.33×10^{-2}

In a second example we solve for a flow around a cylinder who is located inside a pipe. The boundary conditions on the walls are those of a Poiseuille flow. In Figure 5 we show streamlines for a Reynolds number equal to 100. For an exterior problem such flow is unsteady (but still laminar). However for the chosen problem setup the resulting flow is steady.

Figure 5: Flow around a cylinder for Reynolds number 100.

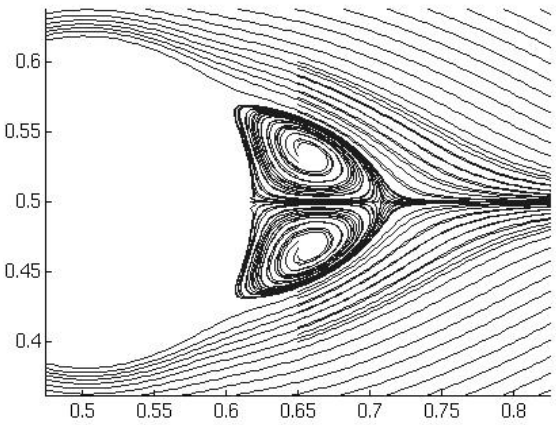

6 Conclusions and extensions

We have presented a second-order accurate solver for the unsteady Navier-Stokes equations on arbitrary geometry domains. We use a hybrid boundary integral, finite element formulation to bypass the need for mesh generation. We employ an efficient double layer formulation for the integral equations. At each time step the method requires two regular grid solves and one integral equation solve.

One restriction of the method, as we have presented it, is the stringent requirements on the regularity of the boundary geometry. However this can be circumvented by replacing the jump computation by direct evaluation. For example the jump terms can be computed to machine accuracy by plugging the exact solution in the stencils that cross the boundary. The exact solution can be obtain by direct evaluation of the velocity using the integral representation. This will require adaptive quadratures—but only for the points close to a corner.

References

Douglas Jr., J. and Russell, T. F. (1982). Numerical methods for convection-dominated diffusion problems based on combining the method of characteristics with finite element or finite difference procedures. *SIAM Journal on Numerical Analysis*, 19(5):871–885.

Gómez, J. and Power, H. (1997). A multipole direct and indirect BEM for 2D cavity flow at low Reynolds number. *Engineering Analysis with Boundary Elements*, 19:17–31.

Greengard, L. and Rokhlin, V. (1987). A fast algorithm for particle simulations. *Journal of Computational Physics*, 73:325–348.

Gunzburger, M. D. (1989). *Finite Element for Viscous Incompressible Flows*. Academic Press.

Mammoli, A. and Ingber, M. (2000). Parallel multipole BEM simulation of two-dimensional suspension flows. *Engineering Analysis with Boundary Elements*, 24:65–73.

Mayo, A. (1984). The fast solution of Poisson's and the biharmonic equations on irregular regions. *SIAM Journal on Numerical Analysis*, 21(2):285–299.

Norburn, S. and Silvester, D. (1999). Fourier analysis of stabilized Q1-Q1 mixed finite element approximation. Numerical Analysis Report 348, The University of Manchester.

Power, H. (1993). The completed double layer integral equation method for two-dimensional stokes flow. *IMA Journal of Applied Mathematics*, 51:123–145.

Power, H. and Wrobel, L. (1995). *Boundary Integral Methods in Fluid Mechanics*. Computational Mechanics Publications.

Pozrikidis, C. (1992). *Boundary Integral and Singularity Methods for Linearized Viscous Flow*. Cambridge University Press.